Geochemistry Geophysics Geosystems G3
AN ELECTRONIC JOURNAL OF THE EARTH SCIENCES
Published by AGU and the Geochemical Society

Article
Volume 7, Number 11
7 November 2006
Q11003, doi:10.1029/2006GC001314
ISSN: 1525-2027

Pyroclastic flow dynamics and hazard in a caldera setting: Application to Phlegrean Fields (Italy)

Micol Todesco
Istituto Nazionale di Geofisica e Vulcanologia, Via D. Creti, 12, I-40128 Bologna, Italy (todesco@bo.ingv.it)

Augusto Neri, Tomaso Esposti Ongaro, and Paolo Papale
Istituto Nazionale di Geofisica e Vulcanologia, Via della Faggiola, 32, I-56126 Pisa, Italy (neri@pi.ingv.it; ongaro@pi.ingv.it; papale@pi.ingv.it)

Mauro Rosi
Dipartimento Scienze della Terra, Università di Pisa, Via S. Maria, 53, I-56126 Pisa, Italy (rosi@dst.unipi.it)

Istituto Nazionale di Geofisica e Vulcanologia, Via della Faggiola, 32, I-56126 Pisa, Italy

[1] Numerical simulation of pyroclastic density currents has developed significantly in recent years and is increasingly applied to volcanological research. Results from physical modeling are commonly taken into account in volcanic hazard assessment and in the definition of hazard mitigation strategies. In this work, we modeled pyroclastic density currents in the Phlegrean Fields caldera, where flows propagating along the flat ground could be confined by the old crater rims that separate downtown Naples from the caldera. The different eruptive scenarios (mass eruption rates, magma compositions, and water contents) were based on available knowledge of this volcanic system, and appropriate vent conditions were calculated for each scenario. Simulations were performed along different topographic profiles to evaluate the effects of topographic barriers on flow propagation. Simulations highlighted interesting features associated with the presence of obstacles such as the development of backflows. Complex interaction between outward moving fronts and backflows can affect flow propagation; if backflows reach the vent, they can even interfere with fountain dynamics and induce a more collapsing behavior. Results show that in the case of large events ($\geq 10^8$ kg/s), obstacles affect flow propagation by reducing flow velocity and hence dynamic pressure in distal regions, but they cannot stop the advancement of flows. Deadly conditions (in terms of temperature and ash concentration) characterize the entire region invaded by pyroclastic flows. In the case of small events (2.5×10^7 kg/s), flows are confined by distal topographic barriers which provide valuable protection to the region beyond.

Components: 9369 words, 10 figures, 4 tables, 2 animations.

Keywords: Phlegrean Fields; multiphase flow; pyroclastic flows; dynamic pressure; volcanic hazard; caldera.

Index Terms: 8414 Volcanology: Eruption mechanisms and flow emplacement; 8428 Volcanology: Explosive volcanism; 8488 Volcanology: Volcanic hazards and risks.

Received 22 March 2006; **Revised** 19 July 2006; **Accepted** 28 July 2006; **Published** 7 November 2006.

Todesco, M., A. Neri, T. Esposti Ongaro, P. Papale, and M. Rosi (2006), Pyroclastic flow dynamics and hazard in a caldera setting: Application to Phlegrean Fields (Italy), *Geochem. Geophys. Geosyst.*, *7*, Q11003, doi:10.1029/2006GC001314.

1. Introduction

[2] The Phlegrean Fields is an active and densely populated volcanic caldera in the urban area of Naples (Figure 1). The caldera formed through the several eruptive events and collapses of different styles and magnitudes which have occurred since the big caldera-forming Campanian Ignimbrite eruption 39 ka ago. The volcanic history of the caldera has been reconstructed in great detail [*Rosi and Sbrana*, 1987; *Orsi et al.*, 2004, and references therein] and mostly comprises explosive events with emplacement of pyroclastic flows, base surges and fallout deposits [*Orsi et al.*, 1996; *Di Vito et al.*, 1999; *Dellino et al.*, 2004a; *Isaia et al.*, 2004]. Hundreds of long periods (years) of intense activity alternated with a few ka periods of eruptive quiescence. About 3.5 ka of quiescence preceded the 1538 AD Monte Nuovo event which led to the formation of a tuff cone in the western part of the caldera [*Di Vito et al.*, 1987; *D'Oriano et al.*, 2005; *Piochi et al.*, 2005]. Since then, extensive fumarolic activity, seismicity, and remarkable episodes of ground deformation [*Barberi et al.*, 1984a] have provided evidence of activity in the caldera, such that the possibility of eruptions in the future cannot be excluded. Given the large number of people presently living within the area, even a small eruption could produce enormous economic consequences, and the volcanic risk for the region is one of the highest in the world. The first attempts to assess volcanic hazard in the Phlegrean region [*Barberi et al.*, 1984b; *Rosi and Santacroce*, 1984] were prompted by two bradyseismic crises (in 1969 and 1982), when the ground rose a few meters in just a few years in possible prelude to an eruption. More recently, several authors have addressed the problem of hazard assessment at the Phlegrean Fields; they have tried to define the location, nature and magnitude of the expected event, and identify areas potentially at risk [*Lirer et al.*, 2001; *Alberico et al.*, 2002; *Dellino et al.*, 2004b; *Orsi et al.*, 2004; *Rossano et al.*, 2004]. Different authors have approached the problem from different perspectives, but there is general consensus on some points: the vent will most likely open within the eastern sector of the caldera (roughly the Agnano plain); activity is expected to be explosive and characterized by pyroclastic density currents (hereafter named pyroclastic flows, in a general sense). The propagation of pyroclastic density currents is therefore one of the issues to be addressed in a comprehensive evaluation of volcanic hazard at the Phlegrean Fields caldera. The dynamics is expected to be complex due to the peculiar topography of the area, which is characterized by a flat ground surface dotted with large and small crater rims, tuff rings and tuff cones. A key issue is whether or not pyroclastic flows could surmount the hills flanking the eastern and northern sides of the caldera and directly threaten the city of Naples.

[3] The assessment of pyroclastic flow hazard involves the identification of areas which are likely to be invaded by pyroclastic flows. In case of an eruption, total devastation is generally assumed to occur in those areas, and complete evacuation appears to be the only possible mitigation measure. Areas at risk have been traditionally identified using maps of past pyroclastic flow deposits, assuming that similar events could occur in the future. *Lirer et al.* [2001], on the basis of the distribution of products during the last 10 ka, suggested that pyroclastic flows and surges would most likely remain confined within the caldera wall. *Orsi et al.* [2004], on the other hand, suggested that flows might spill over the northern rim of the caldera during large events. An attempt to quantify the impact of pyroclastic flows at the Phlegrean Fields was carried out by *Dellino et al.* [2004b]. On the basis of sediment mechanics, and assuming low particle concentrations and quasi-steady, incompressible behavior, these authors estimated local flow densities and shear velocities from structural and textural features of the deposits. *Alberico et al.* [2002] based their estimate of maximum possible run-out on the energy-cone approach [*Sheridan and Malin*, 1983]: they stressed the role of topography in confining flow propagation within the caldera walls, except during large events (VEI 5-6). *Rossano et al.* [2004] came to similar conclusions by computing gravity-driven flow paths on the real topography of the caldera as a function of vent coordinates and of flow rheologies. Although these approaches provide a statistical description of the hazard associated with pyroclastic flows, the application of a 1-D description of the flow to 3-D topography is, in principle, incorrect and introduces uncertainty in the results that cannot be quantified a priori.

2. Aim of the Work

[4] A step forward in the definition of pyroclastic flow impact is based on 2-D and 3-D physical modeling of pyroclastic flow propagation, which has never been applied to the Phlegrean Fields. Models based on the Navier-Stokes equations

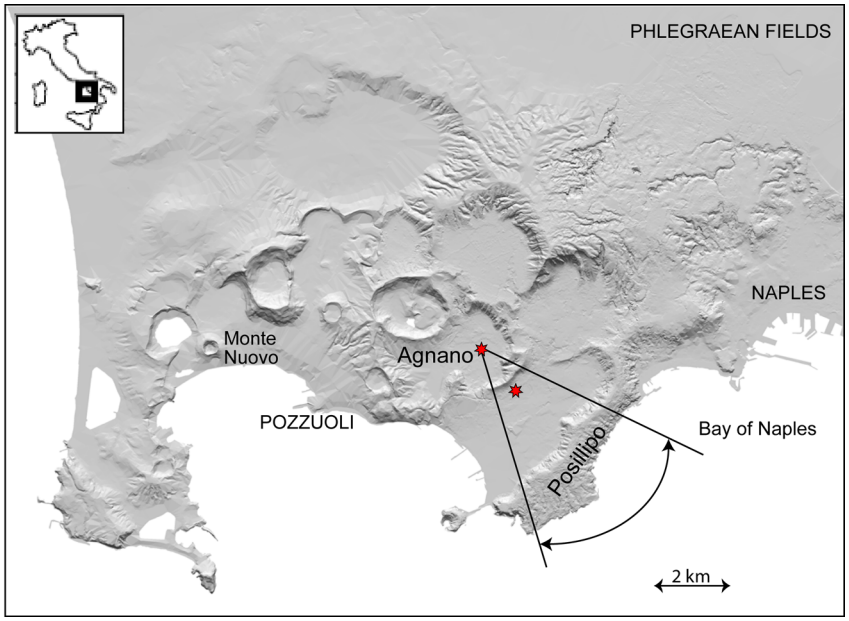

Figure 1. The Phlegrean Fields caldera, with the locations of the Agnano Plain, the Posillipo ridge, and the study area. Stars indicate vent locations for topographic profiles AP and P.

allow the description of relevant flow variables and the quantification of their effects on the involved region. Pyroclastic flows are generally considered very dilute, compressible mixtures of gas and fine particles, for which thermal and mechanical equilibrium can be assumed. Under this assumption, the mixture can be considered a single-phase fluid characterized by bulk properties which depend on particle concentrations [*Córdoba*, 2005; *Ishimine*, 2005; *Suzuki et al.*, 2005]. A more complex approach includes the full description of the multiphase nature of the flow in which particles of different sizes and properties are thermally and mechanically decoupled from the gas phase [*Valentine and Wohletz*, 1989; *Dobran et al.*, 1993; *Neri and Dobran*, 1994; *Neri and Macedonio*, 1996; *Neri et al.*, 2003; *Dartevelle*, 2004; *Dartevelle et al.*, 2004] and which takes into account water phase changes [*Herzog et al.*, 1998; *Oberhuber et al.*, 1998]. In particular, in the present work, the multiparticle PDAC2D model [*Neri et al.*, 2003] was adopted to investigate the generation and propagation dynamics of pyroclastic flows. Comparison of model results with well-studied pyroclastic flow deposits, detailed observation of recent eruptions, and gas-solid laboratory experiments provided a robust semi-quantitative validation of this model, which was shown to be fully consistent with available estimates of flow temperature and velocity, and could appropriately reproduce observed maximum runout, fountain height, and eruptive style [*Neri and Gidaspow*, 2000; *Neri et al.*, 2002; *Clarke et al.*, 2002; *Di Muro et al.*, 2004]. Moreover, several applications of this model allowed identification of important characteristics of pyroclastic flows that are crucial for hazard assessment [*Dobran et al.*, 1994; *Baxter et al.*, 1998; *Todesco et al.*, 2002; *Esposti Ongaro et al.*, 2002]. In this work we address the dynamics of pyroclastic flow propagation in a typical caldera setting, with crater rims and caldera walls rising above an otherwise rather horizontal topography. On the basis of volcanological studies, a number of 2-D eruptive scenarios were selected. Following a well-established practice [*Dobran et al.*, 1994; *Neri et al.*, 1998; *Todesco et al.*, 2002; *Esposti Ongaro et al.*, 2002], flow conditions at the vent were computed by modeling magma ascent along the volcanic conduit for specific magma compositions, reservoir conditions, and eruption intensities. The dispersal of the eruptive mixture into the atmosphere was then simulated to describe the generation and propagation of pyroclastic density currents. For the first time simulations considered three particle types with different physical properties and dimensions representing ash, pumice and crystals, or lithic material found in Phlegrean Fields products. Simulations were performed considering different topographic profiles representative of the southeastern sector of the caldera and accounting for different vent positions with respect to the Agnano rim and Posillipo ridge (see Figure 1). This allowed us to investigate the interaction between a multiphase flow and a simple

topography characterized by the presence of one or two obstacles at different distances.

[5] Results revealed interesting aspects of flow transport and interaction with the obstacles, and suggest that Posillipo does not represent an effective topographic barrier in the case of large-scale events. Hazard flow variables computed by the model were used to estimate the hazard associated with flow propagation along different topographic profiles. In the following sections, we provide a short description of the applied models and some details on the volcanic system and hypothesized eruption scenarios. Selected simulation results are then described and discussed in the conclusions.

3. Modeling Tools and Hazard Variables

[6] The adopted PDAC2D gas-pyroclasts atmospheric dispersal model [*Neri et al.*, 2003] describes the transient, axisymmetric, multiphase flow dynamics of a mixture of N solid particulate phases in a continuous gas phase with M chemical components. In the present simulations, water vapor is the only volatile component assumed in the eruptive mixture, whereas three particle classes are used to represent ash, pumice and lithics. Mass, momentum, and energy balance equations are solved for each phase, including the drag between gas and each particulate phase and among solid particles. Heat exchange between gas and solids is also explicitly computed. Model formulation and solution techniques are fully discussed in several papers published in the international literature [*Dobran et al.*, 1993; *Neri and Dobran*, 1994; *Neri and Macedonio*, 1996; *Clarke et al.*, 2002; *Todesco et al.*, 2002; *Neri et al.*, 2003]. In order to provide the atmospheric dispersal model with realistic boundary conditions at the vent, magma ascent along the volcanic conduit was simulated on the basis of current knowledge of the volcanic system (see next section). In particular, the conduit flow model [*Papale*, 2001] describes an isothermal, one-dimensional, steady flow for a non-equilibrium, two-phase (gas/liquid + crystals) ascending mixture. Magma density and rheological properties are expressed as a function of liquid composition, water concentration, crystal content and temperature. Details on the model formulation and solution techniques are reported in the above-cited reference. We here only recall that the conduit flow model calculates vent diameter and flow conditions for a given mass eruption rate, which are then used as steady boundary conditions at the vent for modeling pyroclastic dispersal. Boundary conditions for the pyroclastic dispersal model also include a no-slip boundary at ground level with no mass outflow and a symmetry axis along the left-hand side of the domain. Note that, although the axisymmetric constraint may lead to underestimation of the turbulent entrainment of atmospheric air into the eruptive column, thereby shifting the transition between Plinian and collapsing style [*Suzuki et al.*, 2005], 2-D simulations still represent a useful trade-off between accuracy and computational efficiency in parametric studies on multiphase flows. Moreover, we focus here on those scenarios characterized by a collapsing regime, in which buoyancy effects are less important. The reported simulations were performed on a 2-D computational domain, with cylindrical symmetry, to better capture the geometry of the sector highlighted in Figure 1. The computational domain extends 6 km in the radial direction and 5 km in the vertical one. Test cases performed on larger domains (up to 10 $\times$ 26 km) confirmed the overall dynamics highlighted by the smaller one. Spatial discretization ranges from 6.5 to 70 m (radially) and from 10 to 100 m (vertically). Such a grid spacing was chosen on the basis of previous experience and following well-known criteria to optimize numerical accuracy. Although a crude simplification of the real three-dimensional topography, the adoption of the simpler, 2-D geometry represents a reasonable first approach to the comprehension of the flow dynamics, and a first step toward the quantification of volcanic hazard that will work as a sound base for future 3-D simulations. Performed simulations provide the spatial and temporal distributions of certain flow variables essential for hazard assessment, such as flow temperature and the concentration of ash in the air. The critical temperature for human survival in the open has been identified as 200°C, whereas the threshold concentration of inhalable particles (<100 μm) is 0.1 kg/m^3 [*Baxter*, 1990; *Baxter et al.*, 1998, 2005; *Esposti Ongaro et al.*, 2002]. Another important flow variable is the dynamic pressure of the flow [*Valentine and Wohletz*, 1989; *Valentine*, 1998; *Esposti Ongaro et al.*, 2002; *Baxter et al.*, 2005]. Following a common approach in wind-engineering [*Cook*, 1985; *Nuovo Colombo*, 1990] based on flow density and velocity, the impact of a pyroclastic flow on urban areas can be estimated in terms of its kinetic energy per unit volume [*Valentine and Wohletz*, 1989; *Valentine*, 1998; *Esposti Ongaro et al.*, 2002]. For a given building type with known characteristics, it is possible to evaluate ranges of dynamic

Table 1. Building Damage Scale for Pyroclastic Flow Impact[a]

Level	Pressure, kPa	Damage
0	<1	none
1	1–3	light
2	2–6	moderate
3	4–10	heavy
4	8–25	partial devastation
5	>25	total devastation

[a] After *Baxter et al.* [2005].

pressures corresponding to different degrees of damage. A damage scale for pyroclastic density currents based on data from nuclear weapons tests was first defined by *Valentine* [1998]. Lower values (Table 1) derive from more recent direct observations of damage caused by pyroclastic surges [*Baxter et al.*, 2005]. According to this new scale, dynamic pressures of 1–6 kPa are capable of generating minor to moderate damage (implosion of windows and the inflow of hot ash which may in turn ignite fires). Values of the order of 10 kPa may lead to heavy damage up to partial devastation, whereas values in excess of 25 kPa cause total devastation with serious damage to even strong earthquake-proof buildings.

[7] Note that the model applied in this study does resolve neither the details of flow interaction with the real ground surface nor the large gradients in flow density and velocity close to the ground due to the 10-m grid resolution. As described in greater detail by *Todesco et al.* [2002], our simulations only describe the flow above the so-called "aerodynamic ground plane," and local effects associated with landforms or with the presence of obstacles are only approximated in terms of average terrain roughness [*Mason*, 1994]. According to this approach, flow variables calculated 5–10 m above the aerodynamic ground plane are extrapolated to estimate average flow dynamics within the interfacial layer [*Cook*, 1985]. In actual fact, there exists an interfacial layer in which the ground surface morphology strongly interact with a stratified flow. As a consequence the dynamic pressure estimates provided in the following should be regarded as first-order values for computing the flow impact and for comparing the effects of different eruptive scenarios.

4. Investigated Volcanic Scenarios

[8] The definition of a scenario entails the characterization of the volcanic event to be simulated (magnitude of eruption, magma temperature and properties, depth of magma reservoir, etc.) and, in this case, also the identification of the vent location.

[9] To define the volcanic event, we referred to the Agnano-Monte Spina (AMS) eruption (the largest event recorded in the last 5 ka) and considered the maximum expected event for this volcanic system [*Orsi et al.*, 2004]. Deposits from this event have been carefully studied [*Rosi et al.*, 1983; *Rosi and Santacroce*, 1984; *Rosi and Sbrana*, 1987; *de Vita et al.*, 1999; *Dellino et al.*, 2001, 2004a; *Papale*, 2004], so that most of the information required to constrain the system is available. The AMS eruption took place 4.1 ka ago and emplaced about 1.2 km^3 of tephra (DRE), leading to the formation of a caldera 3 km in diameter. On the basis of the thickness of deposits, the vent was likely located within the Agnano plain. Petrological data suggest that two isotopically and chemically different magmas (alkali-trachytic and trachytic in composition) fed the eruption and interacted with each other during its last stages. The stratigraphic sequence and textural data suggest that the eruption followed a complex evolution, with alternating magmatic and phreatomagmatic phases sometimes occurring simultaneously. The sequence, characterized by short pauses in eruptive activity, has been divided into 6 members (named A through E [*de Vita et al.*, 1999]) with highly variable lithological features [*Dellino et al.*, 2001]. Eruptive activity emplaced fallout products both inside and outside the Phlegrean Fields caldera. Pyroclastic flows and surges formed due to partial column collapse or as a consequence of phreatomagmatic explosions involving the geothermal system [*de Vita et al.*, 1999; *Dellino et al.*, 2001].

[10] In this work we focus on the magmatic phases of the eruption (B1 and D1) which generated Plinian columns. The estimated heights of these columns, based on the dispersal characteristics of the largest clasts in the deposits, range from 20–23 km (B1) to 22–27 km (D1), depending on the adopted method of calculation. These values correspond to mass flow rates of 2.5×10^7–1×10^8 kg/s for eruptive phase B1, and of 4×10^7–1.8×10^8 kg/s for D1. Pyroclastic flows were generated by partial collapses of the eruptive column, as flow deposits interbedded in fallout products testify. The composition of the two eruptive phases is reported in Table 2. Pre-eruptive temperature and pressure estimates were based on mineralogical assemblages, volatile contents, petrological constraints and considerations deriving

Table 2. Anhydrous Glass of Trachytic Composition From the Agnano Monte Spina Pumices B1 and D1[a]

	SiO_2	TiO_2	Al_2O_3	Fe_2O_3	FeO	MnO	MgO	CaO	Na_2O	K_2O	X Vol. %
B1	61.26	0.38	18.38	1.17	2.33	0.14	0.74	2.97	4.58	8.04	28
D1	60.86	0.39	18.27	1.29	2.59	0.12	0.90	2.96	4.12	8.50	36

[a] Expressed in wt% of 10 major oxides [*Romano et al.*, 2003] and volumetric fraction of crystal content (X).

from modeling of multicomponent liquid-gas equilibria. Accordingly, magma temperatures of about 830°C (1100°K) and 900°C (1170°K) were considered for units B1 and D1, respectively, and a volcanic conduit of 4 km was inferred [*Papale*, 2004]. Given the uncertainties associated with the definition of the initial water content dissolved in the magma and the importance of this parameter in defining the eruptive style, two different values (4 and 3 wt%) were considered.

[11] To define the grain-size and density of solid particles, a required input for models, standard and novel sedimentological analyses were carried out on samples from the two considered eruptive units. Samples are representative of deposits from pyroclastic flows of limited spatial extent generated by the collapse of the volcanic column and found between B1 and D1 fallout products. Grain-size and component analysis allowed the identification of three main types of pyroclasts with different properties: pumice, ash and loose solid material (lithics and crystals) (Table 3). The ash content in the eruptive mixture was obtained by adding the ash content found in the pyroclastic flow deposit and the amount of ash elutriated during pyroclastic flow emplacement, taking into consideration the elutriation factor proposed by *Walker* [1981]. Far from being an accurate representation of particle distribution at the vent or in the flow deposits, this analysis provided a first-order approximation of main grain-size populations to be considered in our models. In the described simulations, each particle type was represented by spherical particles of uniform size corresponding to the particle diameter (Table 3) having the same volume/surface ratio as the original distribution [*Kunii and Levenspiel*, 1995].

[12] Last, to complete the eruptive scenario, the vent location had to be identified. As mentioned earlier, the vent could probably open in the Agnano plain [*Orsi et al.*, 2004]. To deal with its uncertain location, we performed simulations considering different topographic profiles corresponding to the southeastern sector of the Agnano Plain (Figure 1). The first topographic profile (Profile AP) assumes a vent located in the middle of the Agnano plain and therefore involves two obstacles: the rim of the Agnano caldera (110 m high, 950 m from the vent) and the Posillipo ridge (160 m high, 3400 m from the vent). The second profile (Profile P) represents the same sector, but with a vent opening on the Agnano crater rim. The only obstacle along this second profile is therefore the Posillipo ridge (160 m, 2500 m from the vent). A third, flat topography was then considered for comparison (Profile F). Simulations performed with the pyroclastic density current model are listed in Table 4.

5. Simulation Results

5.1. Large Events: Overall Dynamics (Simulation B1-AP-L)

[13] The first simulation (B1-AP-L) describes the evolution of a large-scale event during which the eruptive phase B1, with an initial water content of 4 wt%, is discharged along profile AP, characterized by two topographic obstacles. The evolution of this simulation is represented in Figures 2a and 2b, where gas temperatures and velocities are shown at different times. As the simulation begins, the eruptive mixture injected into the atmosphere forms an eruptive column above the vent. Local instabilities develop in the fountain, as a result of the competing effects of vertical momentum in the gas thrust region, buoyancy, enhanced by air entrainment, and gravity. As a result, two radially spreading, suspended flows develop both at the top of the column (~1800 m) and at lower elevations (~500 m). After 72 s, the lower suspended flow collapses and hits the ground right on top of

Table 3. Particle Size, Density, and Volumetric Fraction for the Two Considered Eruptive Phases

Eruptive Phase	Particle Type	Particle Size, μm	Density, kg/m^3	Initial Volume Fraction
B1	Pumice	350	700	0.0480
	Ash	10	2400	0.0163
	Crystal + lithics	190	3000	0.0064
D1	Pumice	280	530	0.0272
	Ash	10	2400	0.0235
	Crystal + lithics	215	3000	0.0134

Table 4. Eruptive Phase, Vent Conditions, and Topographic Profile for the Simulations of Pyroclastic Flow Propagation[a]

Simulations	Phase	M, kg/s	H_2O, wt%	T, °K	D, m	V, m/s	ε_g	P, MPa	O
B1-AP-L	B1	1×10^8	4	1100	107	127	0.9293	1.152	AP
B1-AP-S	B1	2.5×10^7	3	1100	75	110	0.9595	0.51	AP
D1-AP	D1	1.8×10^8	4	1170(1100)	133	121	0.9359	1.357	AP
D1-P	D1	1.8×10^8	4	1170	133	121	0.9359	1.357	P
D1-F	D1	1.8×10^8	4	1170	133	121	0.9359	1.357	-

[a] M, eruption intensity; H_2O, water content; T, temperature of eruptive mixture; D, conduit diameter; V, mixture velocity; ε_g, gas volumetric fraction; P, pressure; O, topographic obstacles (A, Agnano; P, Posillipo).

Agnano. A portion of the eruptive mixture flows back toward the vent, while the rest forms a pyroclastic flow that propagates outward. The subsequent evolution is highly unsteady: the column collapse height changes through time, and the point where the collapsing material hits the ground also shifts from the top of the Agnano rim to more proximal locations. As a consequence, feeding of the pyroclastic flow is rather discontinuous, with eruptive material sometimes mostly driven toward the fountain where it favors a more collapsing behavior, and other times substantially contributing to flow advancement.

[14] After 136 s, the flow has reached the distal hill, and temperatures in the region between the two obstacles are as high as 600°C (Figures 2a and 2b). The presence of the distal obstacle reduces the flow velocity without stopping it completely. Further column collapses significantly thicken the flow and facilitate its advancement beyond the Posillipo ridge. As the flow moves uphill deceler-

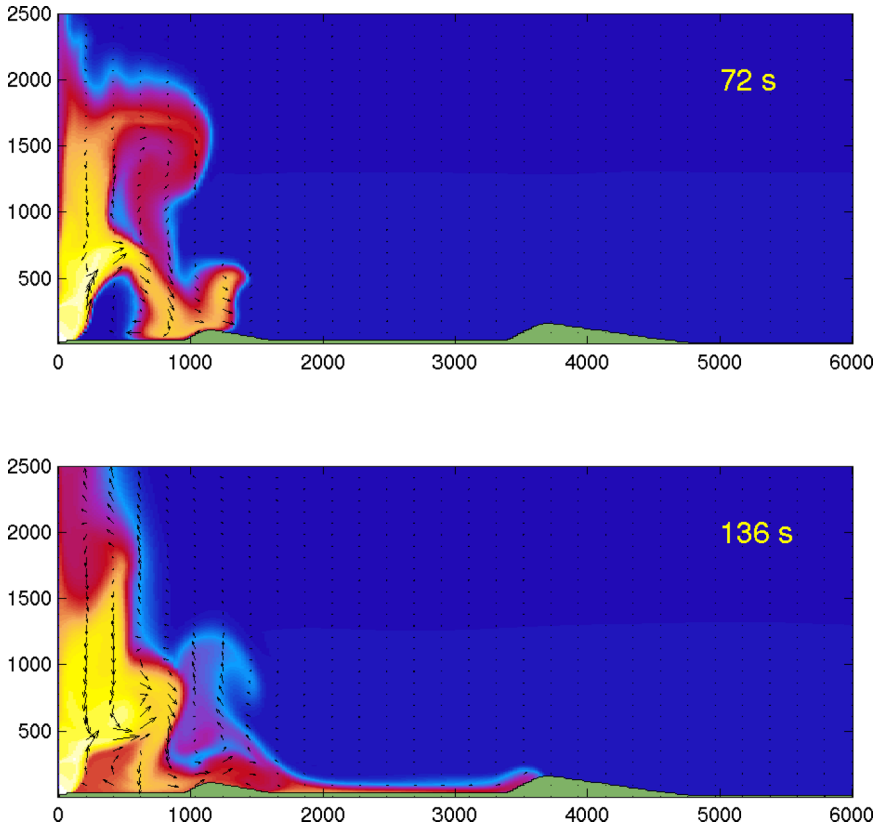

Figure 2a. Simulation B1-AP-L. Gas temperature (colors) and velocity field (vectors) after 72 and 136 s of simulation. Maximum gas velocity (longest arrows) changes slightly in different plots, ranging from 296 to 308 m/s. Topographic profile with two obstacles, representing the Agnano crater rim and Posillipo. The entire evolution of the temperature field is shown in Animation 1 provided as dynamic content.

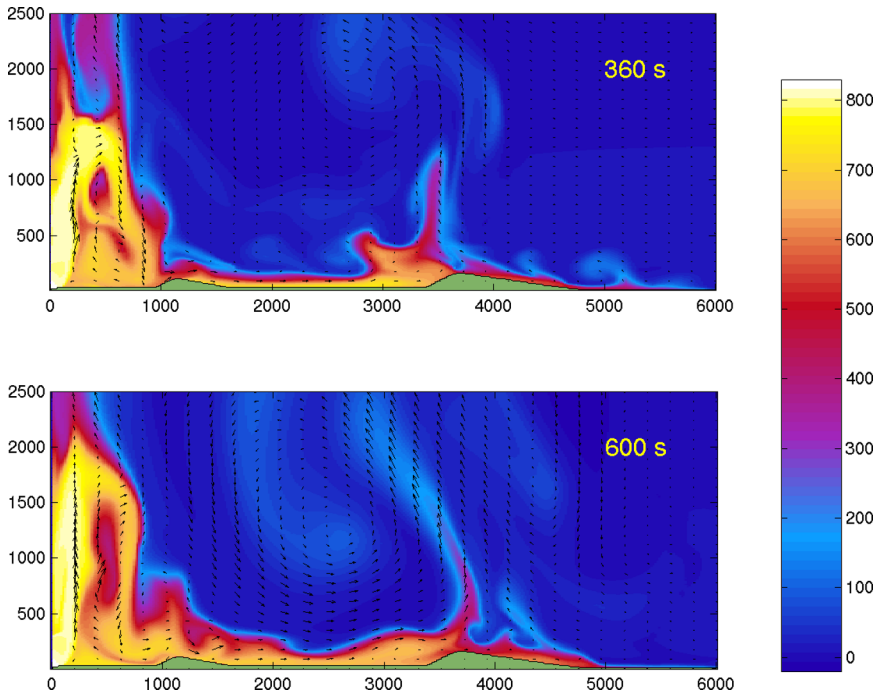

Figure 2b. Simulation B1-AP-L. Gas temperature (colors) and velocity field (vectors) after 360 and 600 s of simulation. Maximum gas velocity (longest arrows) changes slightly in different plots, ranging from 296 to 308 m/s. Topographic profile with two obstacles, representing the Agnano crater rim and Posillipo. The entire evolution of the temperature field is shown in Animation 1 provided as dynamic content.

ating, hot gases segregate upwards dragging a portion of solid particles to form a small phoenix cloud (360 s). A thin pyroclastic flow head can surmount the obstacle and propagate downslope, covering a distance of 6 km in about 300 s. Continuous feeding of the pyroclastic flow increases temperatures considerably, so that those between the two hills are as high as 700°C. Lower values still well above the critical threshold are found beyond the distal hill (5 km), where the thin flow may attain temperatures of 450°C. At this location, short-term temperature attenuation may occur as a consequence of discontinuous feeding of the flow beyond the obstacle, and due to the strong vent-ward winds which favor air entrainment and cooling. Nevertheless, at the end of the simulation (600 s), high temperatures (450–650°C) are observed along most of the computational domain.

[15] Even if the distal hill does not stop flow propagation, not all the eruptive material can surmount the obstacle: a fraction accumulates at the base of the hill and forms a particle-rich, ground-hugging layer which, under favorable conditions, may propagate backward toward the vent and interact with new flow fronts (Figure 3). Outward moving pyroclastic flows can either stop the propagation of the backflow or incorporate the backflow, dragging particles back toward the hill, or they can flow over the particle-rich layer without stopping its backward motion. Prevailing flow directions at different times and locations depend on the relative size, velocity and density of the forward- and backward-moving flow fronts. The obstacle also affects the distribution of different solid particles. Figure 3 illustrates velocity fields and volumetric fractions of pumice, ash, and lithics after 300 s of simulation. Different solid particles tend to accumulate along the ground and in front of the obstacle, but because of their different properties, their relative proportion at ground level changes with time and location. Heavier lithics are preferentially concentrated in the particle-rich layer that forms in front of the obstacle, whereas lighter pumice and ash particles easily enter phoenix clouds when they form.

[16] Results from numerical simulations can also be analyzed in terms of hazard flow variables. As mentioned in the previous section, a first-order estimate of the impact of pyroclastic flows on buildings is given by the dynamic pressure of the flow. The time-wise evolution of dynamic pressure for this simulation (Figure 4a) reflects the complex dynamics of the eruption, characterized by discontinuous feeding of the flow with peak values

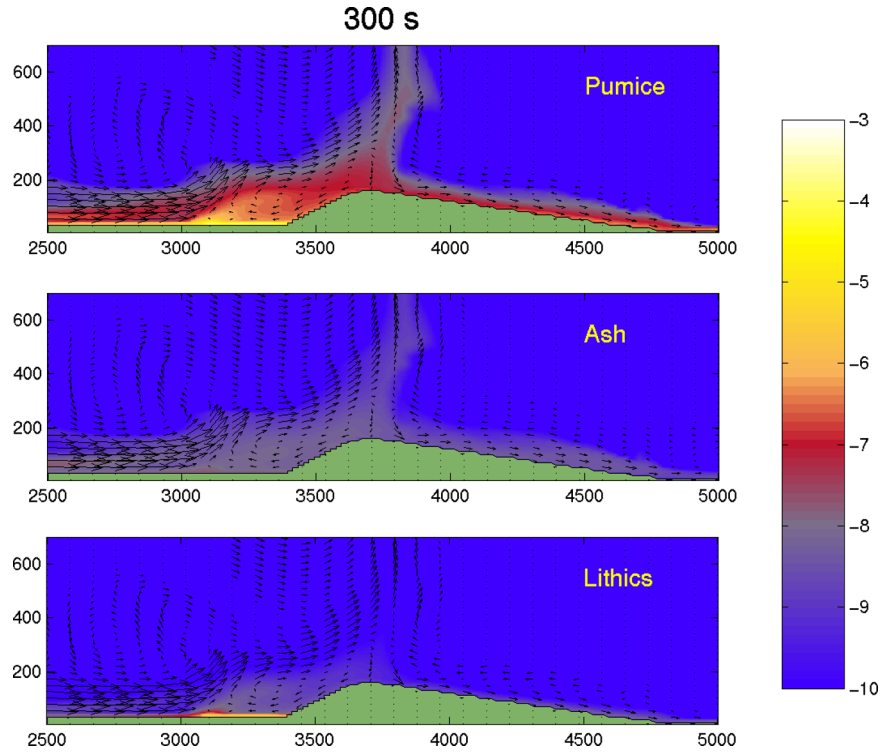

Figure 3. Simulation B1-AP-L. Detail of the volumetric particle fraction (log scale) of pumice, ash, and lithics at the base of Posillipo after 300 s of simulation. The velocity field is also shown (longest arrows represent the maximum particle velocity, here about 60 m/s).

generated by periodic column collapses. At a distance of 2500 m from the vent, the first flow front is associated with a dynamic pressure of about 1 kPa. Further column collapses generate more energetic flows, and after 320 s the dynamic pressure at this location reaches a maximum value of 3.6 kPa. These values are associated with high horizontal flow velocities at this location (up to 30 m/s, Figure 4b). Note that the last peak (1.4 kPa, after 476 s) is generated by the passage of a backflow propagating from the base of the Posillipo hill toward Agnano, with a negative (i.e., directed toward the vent) horizontal velocity of 9 m/s (Figure 4b). Its arrival at this location is marked by a significant increase in the density of the mixture (Figure 4c), which determines an increase in the dynamic pressure.

[17] The flow velocity is much lower 3300 m from the vent due to the presence of the obstacle. After an initial peak of about 10 m/s when the first flow front reaches this location, the horizontal flow velocity then becomes nearly negligible. Continuous changes in flow direction are recorded as new flow fronts arrive and backflows are generated, but absolute values are commonly close to zero. As a consequence, dynamic pressure never exceeds 0.5 kPa at this location, despite the large increment in mixture density (up to 43 kg/m^3) associated with particle sedimentation at the base of the obstacle. A significant drop in density occurs at the end of the simulation, when backflows remove material from this location.

[18] The first flow front that passes over the hill reaches the third location (5000 m from the vent) after 228 s of simulation. At this time, the flow velocity there is close to 20 m/s thanks to the favorable slope, but it is associated with a very low mixture density (4 kg/m^3). The resulting dynamic pressure (0.6 kPa) is higher than along the ventward slope of the ridge, but it still below the threshold associated with light damage (Table 1). Afterwards, discontinuous feeding and ventward winds determine lower flow velocities, such that dynamic pressures remain below 0.35 kPa.

[19] Gas temperature represents another important hazard variable (Figure 4d). In areas invaded by pyroclastic flows this value is commonly above the critical threshold for human survival, but temperature effects on buildings, and on the people inside shelters, vary considerably in relation to the length of exposure to extreme heat. Figure 4d shows how the arrival of a flow causes an immediate increase

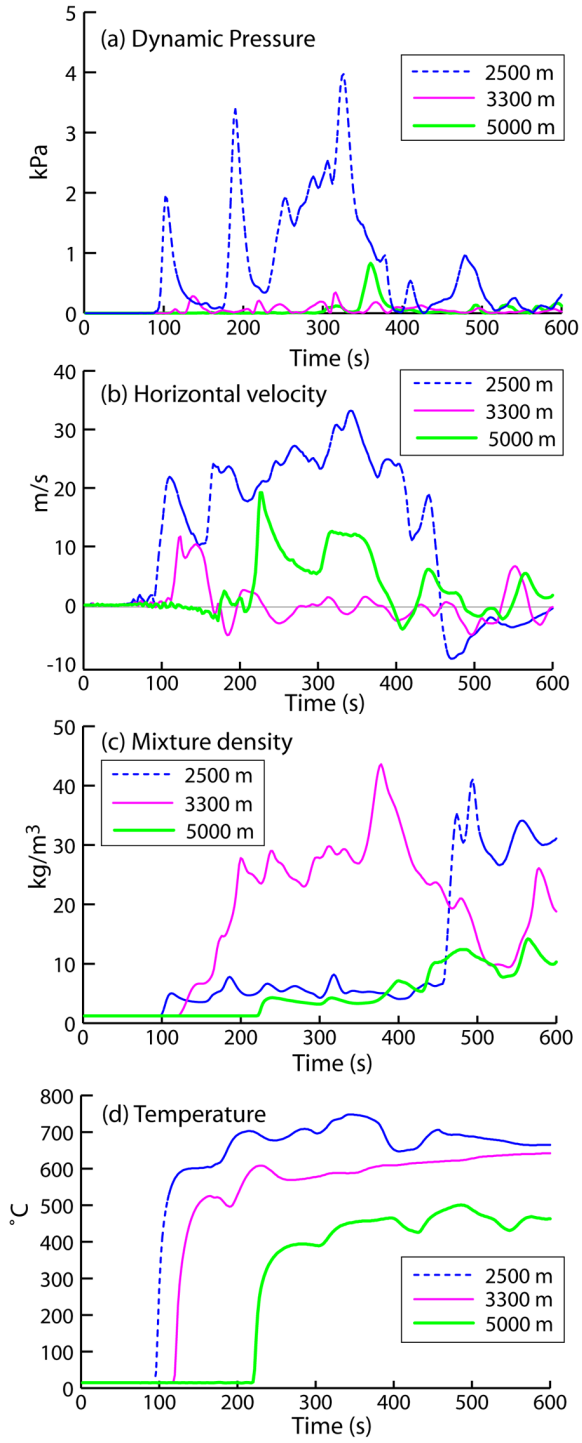

Figure 4. Simulation B1-AP-L. Time-wise distribution of hazard flow variables at ground level and at different distances from the vent: between the hills (2500 m); at the base of Posillipo (3300 m); and beyond Posillipo (5000 m). (a) Dynamic pressure (kPa); (b) flow velocity (m/s); (c) density of the eruptive mixture (kg/m^3); and (d) gas temperature (°C). Details of flow propagation between the obstacles, and associated dynamic pressure changes, are shown in Animation 2 provided as dynamic content.

in temperature to extreme values which are maintained throughout the simulation. Up to 3300 m from the vent temperatures can reach 600°C. Beyond the hill, temperatures are only slightly lower (400–500°C) and remain rather constant, with only minor fluctuations associated with discontinuous flow feeding and air entrainment.

[20] The third hazard variable associated with pyroclastic flow propagation is the concentration of inhalable particles (<100 μm). In the simulations presented here, the only inhalable particle type is ash. The critical ash concentration roughly corresponds to a volumetric fraction of 4×10^{-5}. This value is generally exceeded by one order of magnitude everywhere in this simulation (not shown), even though at distal locations large oscillations may temporarily drive ash fractions below this threshold limit.

5.2. Small Events: Overall Dynamics (Simulation B1-AP-S)

[21] A few simulations were performed considering a smaller mass eruption rate (2.5×10^7 kg/s). Initial water contents of 4 and 3 wt% were considered, and simulations were performed along the three topographic profiles presented above. In all cases, flows are characterized by shorter runouts and are not capable of overriding the Posillipo ridge.

[22] We here only describe the simulation performed along the AP profile with an initial water content of 3 wt%. Figure 5 shows the temperature distribution and velocity fields at three different moments during the simulation. As in the case of the larger event, an eruptive column develops and collapses shortly thereafter. In this case, however, the eruptive material hits the ground closer to the vent, in front of the Agnano rim (60 s). As the flow propagates radially, the rim represents a first and very close obstacle which does not stop but hinders flow advancement. The low water content favors the collapsing behavior, thereby ensuring a continuous feeding of the flow, which contributes to its propagation. As the first obstacle is overcome, a fraction of the eruptive mixture slides back toward the vent, forming a small and proximal backflow. A thin flow propagates outward, and small phoenix clouds are generated as the flow velocity declines with distance from the vent. After about 300 s, the Posillipo ridge is finally reached. The flow, however, does not have enough energy to climb the slope, and a thin backflow forms at the base of the obstacle. The overall dynamics lead to the devel-

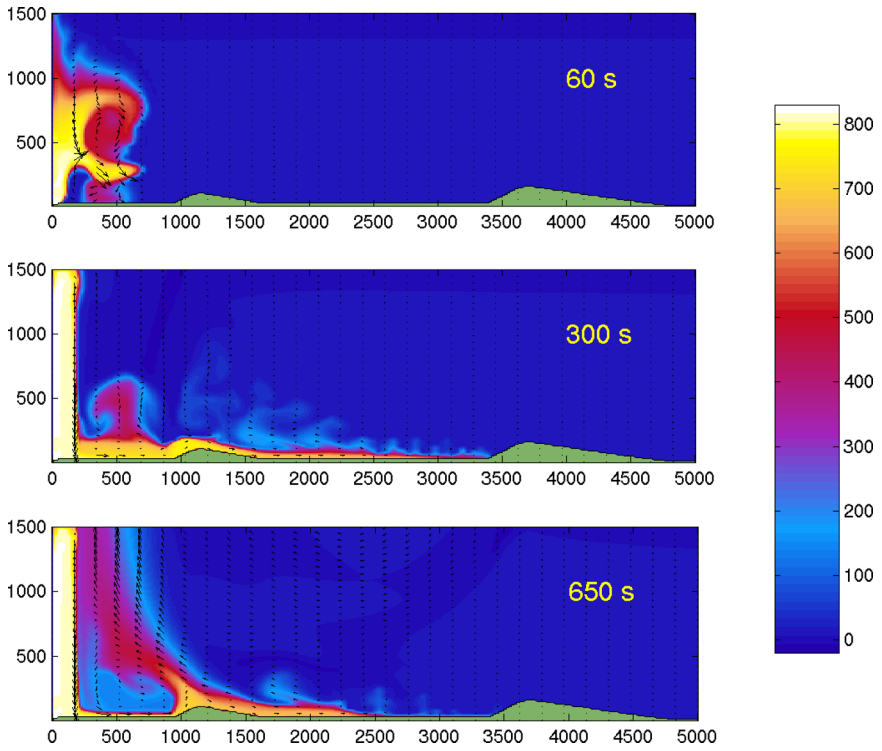

Figure 5. Simulation B1-AP-S. Gas temperature (colors) and velocity field (vectors) after 60, 300, and 650 s of simulation. Maximum flow velocity ranges from 214 m/s (60 s) to 196 m/s (300 and 650 s). Topographic profile with two obstacles representing the Agnano crater rim and Posillipo.

opment of winds which blow toward the vent and drag the phoenix cloud toward the fountain (650 s). The simulation runs for 1000 s, but the flow is never capable of surmounting the distal obstacle. Conditions between the two hills remain deadly due to high temperatures (400–700°C) and ash contents above the critical threshold; lower flow velocities produce a dynamic pressure of ~1 kPa.

5.3. Large Events: Role of Topography (Simulations D1-AP, D1-P, D1-F)

[23] Other simulations were performed considering the D1 eruptive unit. This unit is characterized by a mass eruption rate of 1.8×10^8 kg/s, a slightly higher eruption temperature (~900°C), and a lower particle fraction containing less pumice than eruptive unit B1. A simulation with an eruptive mixture temperature of ~830°C was also performed to allow comparison with simulation B1-AP-L. The evolution along profile AP is qualitatively similar to the one described for eruptive phase B1: subsequent column collapses feed pyroclastic flows that propagate outward, finally overriding the Posillipo ridge. Phoenix clouds form as the flow decelerates, and backflows are generated down the ridge slope. In this case, the larger mass flow rate at the vent generates a wider eruptive column and a thicker pyroclastic flow that propagates somewhat faster than in simulation B1-AP-L. Backward motion is restricted by the nearby Posillipo ridge, as the continuous generation of new and fast flow fronts hinders the propagation of backflows toward the more proximal locations. Figure 6 compares dynamic pressures at ground level, 2500 m from the

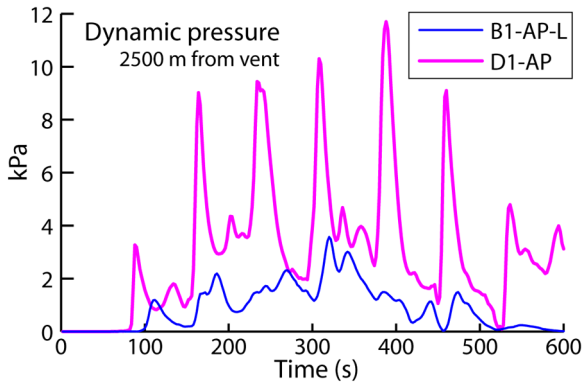

Figure 6. Temporal evolution of dynamic pressure (kPa) in simulations B1-AP-L and D1-AP (both run with an eruptive mixture temperature of 830°C). Reported values refer to ground level and to a distance of 2500 m from the vent.

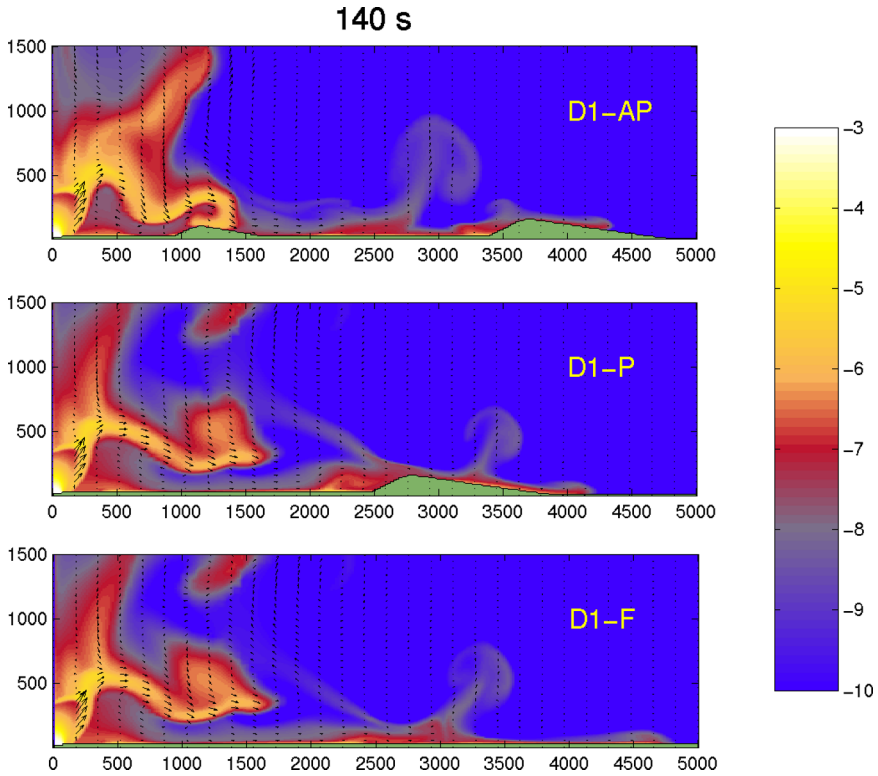

Figure 7a. Gas temperature (colors) and velocity field (vectors) after 140 s along three different topographic profiles: with two obstacles (simulation D1-AP), with one obstacle (D1-P), and flat (D1-F). Maximum gas velocity ranges from 307 m/s (D1-AP) to 309 m/s (D1-F).

vent, for simulations D1-AP and B1-AP-L, both at 830°K. In both cases, peak values correspond to the arrival of new flow fronts generated by column collapses. The larger mass flow rate in simulation D1-AP generates faster flows (up to 55 m/s) with respect to simulation B1-AP-L and therefore higher dynamic pressures (up to 11.7 kPa). A larger number of column collapses (and associated pyroclastic flow arrivals) also characterize the larger D1-AP event.

[24] Simulations performed with a higher initial temperature (900°C) were run along three different topographic profiles: one with two obstacles, as in the previous case (profile AP); one with the Posillipo ridge only (profile P), and a third, flat profile for comparison (profile F). The impact of obstacles is strictly in relation to their distance from the vent. Distal obstacles generally hinder flow propagation by reducing flow velocity and inducing particle sedimentation. Closer obstacles may interfere with the column dynamics: if the eruptive mixture hits the ground along the Agnano inner slope or closer to the vent the crater rim will act as a barrier, driving most of the eruptive material toward the vent, where it will interfere with the discharge of new material and induce a more collapsing behavior. In contrast, if the collapse occurs beyond the top of the rim, outward propagation will be enhanced by the rim slope.

[25] The initial evolution is similar in the three simulations: an eruptive column forms and reaches a height of about 2300 m, where it begins to spread out, forming a suspended flow 500 m above the surface. After 70 s this flow collapses, hitting the ground 1–1.5 km from the vent. This corresponds to the position of the Agnano hill along the AP profile: the slope accelerates the outward, downhill propagation of the flow. As a result, the pyroclastic flow that forms along this profile is initially the fastest. Figure 7a illustrates flow propagation along the three different profiles after 140 s of simulation. At this time, the distal obstacle has been reached and overcome, causing a deceleration of the flow along both profiles AP and P. The most advanced pyroclastic flow head is now the one propagating along the flat topography. However, the flow along AP maintains the advantage gained down the slope of the proximal hill, and it is still ahead of the flow along profile P. Sedimentation is favored in front of the distal obstacle, where small backflows form, but their full development is prevented by the continuous arrival of new flow fronts discharged

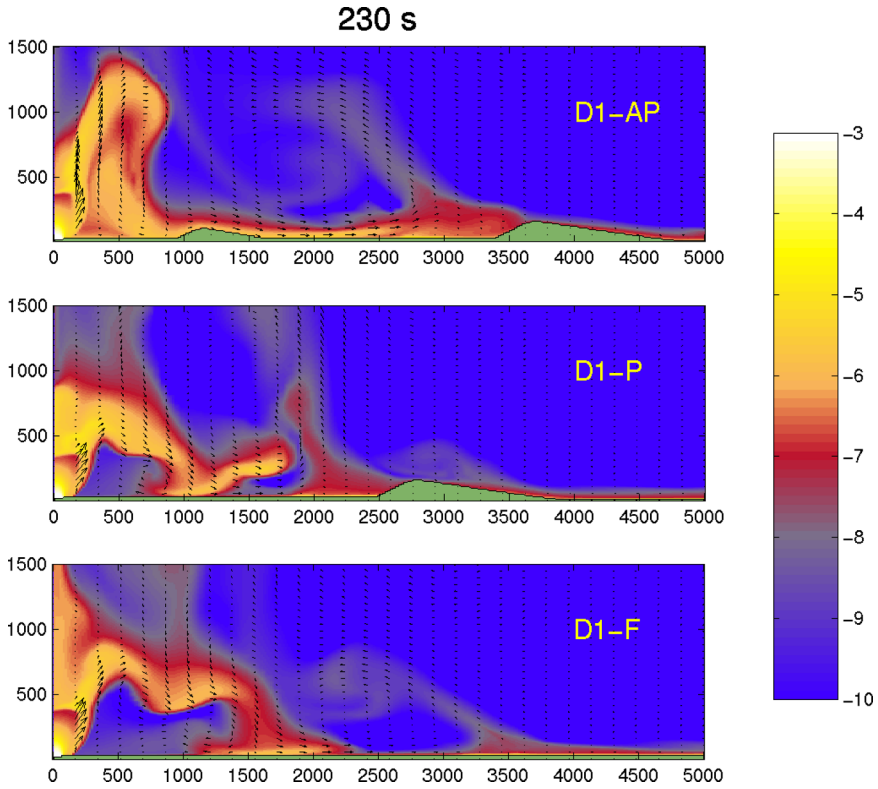

Figure 7b. Gas temperature (colors) and velocity field (vectors) after 230 s along three different topographic profiles: with two obstacles (simulation D1-AP), with one obstacle (D1-P), and flat (D1-F). Maximum gas velocity ranges from 307 m/s (D1-AP) to 309 m/s (D1-F).

by the fountain. Phoenix clouds form every time the flow decelerates and are a common feature in all three simulations. At this time, it is interesting to note that the fountains feeding the flows along profile P and F are almost identical, whereas the one along profile AP differs somewhat because it is affected by the proximal obstacle. Later, as the effects associated with the distal ridge propagate all the way to the vent region, profiles P and F also show different fountain dynamics. Figure 7b describes a column collapse in the three simulations after 230 s: the timing and point of impact differ in the three cases. A newly formed pyroclastic flow is approaching along profile AP where, at this time, the fountain is discharging material within the Agnano crater rim. Along profile P collapsing material is just hitting the ground 1 km from the vent, whereas along the flat profile the collapse has already occurred 1.5 km from the vent. The absence of obstacles along profile F favors flow propagation, and a particle-rich layer forms more than 3 km from the vent. At the end of all three simulations (not shown), pyroclastic flows cover the entire region within a radius of 5 km, and ground temperatures reach up to 800°C. Ash concentrations are also above the critical threshold for human survival.

[26] Different topographic profiles are also associated with different values of dynamic pressure. In Figure 8, the time-wise distribution of dynamic pressure at ground level is shown at two different locations (2 and 5 km from the vent) for the three considered profiles. As mentioned above, the presence of a proximal obstacle accelerates flow propagating downhill and favors the collapse of the fountain. As a result, dynamic pressures along profile AP, 2 km from the vent, are high (up to 22 kPa) and peak repeatedly. Similar but lower peaks are also found along the flat topography at the beginning of the simulation. As time goes by, however, differences in the evolution of the two simulations increase: after 400 s of simulation, peaks in the dynamic pressure along profile AP progressively decline, whereas values along profile F increase up to the maximum value of 25 kPa.

[27] If only one distal obstacle is present, its overall effect is to reduce the dynamic pressure recorded 2 km from the vent. Backflows that form in front of the obstacle interact with new propagating fronts,

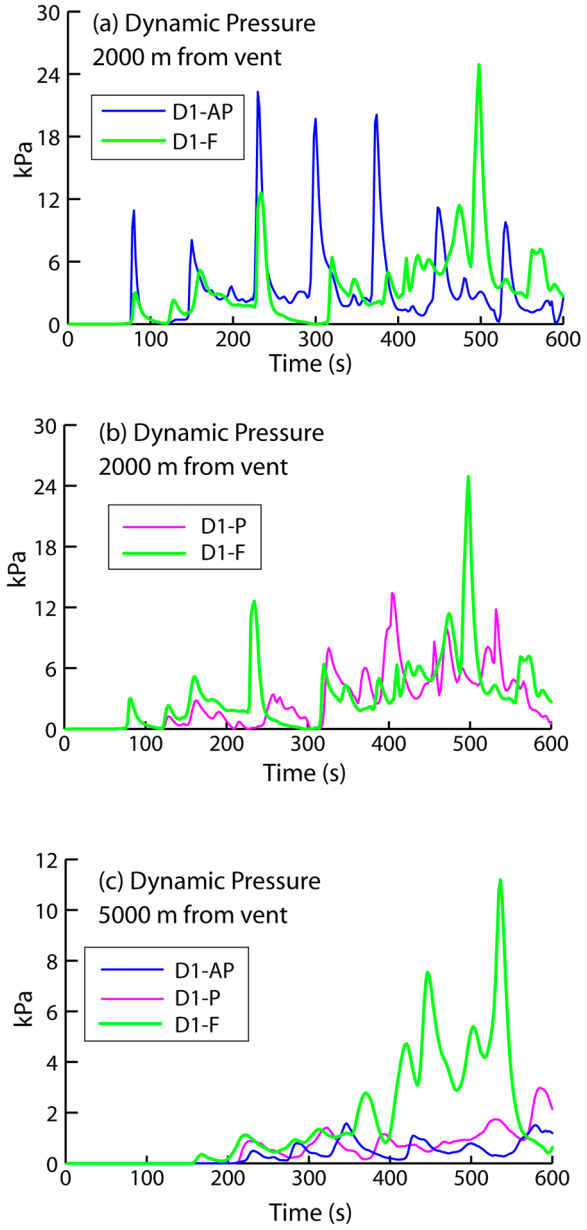

Figure 8. Temporal evolution of dynamic pressure (kPa) at ground level along different topographic profiles: (a) simulations D1-AP and D1-F, 2000 m from the vent; (b) simulations D1-P and D1-F, 2000 m from the vent; and (c) simulations D1-AP, D1-P, and D1-F, 5000 m from the vent, beyond the obstacles. Maximum gas velocity ranges from 304 m/s (D1-AP) to 312 m/s (D1-F).

reducing their velocity well before the obstacle. With respect to the flat topography, dynamic pressures (up to 13 kPa, 406 s) are therefore lower at this location.

[28] At a distal location (5 km), the sheltering effect of obstacles is more evident: dynamic pressures do not exceed 1.5 kPa along profile AP and 3 kPa along profile P. Note that dynamic pressures for these two profiles do not differ much at this location, suggesting that the proximal obstacle only plays a minor role. Attenuation of the flow impact is also observed along the flat profile due to the distance from the vent: the maximum dynamic pressure at this location (11 kPa) is less than half that observed at 2 km.

6. Conclusions

[29] In this work we addressed the problem of pyroclastic flow propagation in a typical caldera setting, where crater rims may hinder flow advancement. In particular, our application focused on the southeastern sector of the Phlegrean Fields caldera, where the Posillipo ridge could possibly protect the town of Naples. Simulations are based on the definition of the volcanic system that fed the Agnano-Monte Spina eruption, which was taken here as a reference case history. Magma ascent along the volcanic conduit was simulated in order to calculate appropriate conditions at the vent. Dispersion of the eruptive mixture into the atmosphere was simulated on a 2-D, axisymmetric domain for set vent conditions. Modeling results describe the development of a collapsing volcanic column and the generation and propagation of pyroclastic density currents. Different magma compositions, water contents, mass eruption rates, and topographic profiles, all consistent with data on the AMS eruption, were considered in the different scenarios. Performed simulations reveal some interesting features of pyroclastic flow propagation along a flat ground surface with one or two concentric crater rims.

[30] In agreement with previous results [*Todesco et al.*, 2002], simulations suggest that eruption intensity is the main parameter controlling the propagation of pyroclastic flows. In the present application, large events ($\geq 10^8$ kg/s) generate pyroclastic flows which are thicker and faster, and which overrun topographic obstacles more easily, covering larger distances. In contrast, flows generated by small scale events (2.5×10^7 kg/s) are fully confined by the distal ridge, even when considering low initial water contents (3 wt%) which favor column collapse.

[31] In addition, simulations showed how the presence of obstacles affects flow propagation in several ways. Obstacles directly modify the flow velocity, which decreases on the ventward slope

of the hill and increases again whenever the flow can surmount the obstacle and propagate outward, downhill. Every time the flow decelerates, hot gases and light particles decouple from the flow and rise to form phoenix clouds, thereby contributing to flow deceleration.

[32] As the flow propagates uphill, a portion of material segregates at the base of the flow and eventually slides back downward, generating backflows that propagate toward the vent. These backflows, already identified in the field [*Fisher*, 1990; *Ort et al.*, 2003], represent another important feature (along with obstacles) affecting the outward propagation of flows. Interaction between new flow fronts and backflows certainly generates complex and interesting depositional features. Although the interpretation of modeling results in this respect is beyond the scope of the present paper, if properly investigated these features could provide elements for interpreting eruptive sequences in the field.

[33] If the obstacle is close to the vent, as is the Agnano crater rim in our simulations, backflows may enter the vent region and interfere with the fountain dynamics. As a result, the presence of a proximal obstacle, instead of providing some kind of protection to the surrounding regions, promotes collapse events and more continuous feeding of pyroclastic flows. The resulting dynamic pressure is therefore higher and characterized by a larger number of peaks. On the other hand, the presence of two concentric crater rims reduces dynamic pressures in the distal region down to values corresponding to only light damage according to the scale of *Baxter et al.* [2005]; it may also prevent flow propagation in the case of small eruptions. The presence of obstacles does not in any way attenuate temperatures or the distribution of particle fractions, which in the case of large events reach and maintain values well above survival thresholds, even beyond the hills.

[34] Our results suggest that in the case of large events distal obstacles as high as the Posillipo hill do not protect the area beyond. This finding is not new in the literature, but it is for the first time based on quantitative results from a realistic description of the involved physical processes. As the model does not account for the real 3-D topography, our calculation of dynamic pressure at different locations only represents a first order estimate of the impact associated with a given scenario; it should be considered a starting point for detailed pyroclastic flow hazard assessment in the area. The 3-D version of the model has already been developed and is being tested on the Vesuvius [*Cavazzoni et al.*, 2005; *Esposti Ongaro et al.*, 2006; T. Esposti Ongaro et al., A parallel multiphase flow code for the 3D simulation of explosive volcanic eruptions, submitted to *Parallel Computing*, 2006]. The application of 3-D models which account for the real caldera topography will therefore be possible in the near future. The physical model, however, does not allow full hazard assessment, as it does not provide any information on the actual probability associated with the simulated phenomenon. Numerical modeling represents an important contribution to hazard assessment, which requires the availability and integration of multidisciplinary data.

Acknowledgments

[35] This work was carried out within the framework of GNV Project 17 (2001–2003 Framework Program) and of the V3-Campi Flegrei Project funded by the Italian Department of Civil Protection. The authors wish to thank George Bergantz and an anonymous reviewer for their comments on the manuscript.

References

Alberico, I., L. Lirer, P. Petrosino, and R. Scandone (2002), A methodology for the evaluation of long-term volcanic risk from pyroclastic flows in Campi Flegrei (Italy), *J. Volcanol. Geotherm. Res.*, *116*, 63–78.

Barberi, F., G. Corrado, F. Innocenti, and G. Luongo (1984a), Phlegrean Fields 1982–1984: Brief chronicle of a volcano emergency in a densely populated area, *Bull. Volcanol.*, *41*, 1–22.

Barberi, F., F. Innocenti, G. Luongo, M. Rosi, R. Santacroce, and R. Scandone (1984b), Il rischio vulcanico nei Campi Flegrei, CNR-GNV report, Gruppo Naz. per la Vulcanol., Cons. Naz. delle Ric., Rome.

Baxter, P. J. (1990), Medical effects of volcanic eruptions: I, Main causes of death and injury, *Bull. Volcanol.*, *52*, 532–544.

Baxter, P. J., A. Neri, and M. Todesco (1998), Physical modeling and human survival in pyroclastic flows, *Nat. Hazards*, *17*, 163–176.

Baxter, P. J., R. Boyle, P. Cole, A. Neri, R. Spence, and G. Zuccaro (2005), The impact of pyroclastic surges on buildings at the eruption of the Soufrière Hills volcano, Montserrat, *Bull. Volcanol.*, *67*, 292–313.

Cavazzoni, C., T. Esposti Ongaro, G. Erbacci, A. Neri, and G. Macedonio (2005), High performance computing simulations of pyroclastic flows, *Comput. Phys. Comm.*, *169*, 454–456.

Clarke, A., B. Voight, A. Neri, and G. Macedonio (2002), Transient dynamics of vulcanian explosions and column collapse, *Nature*, *415*, 897–901.

Cook, N. J. (1985), *The Designer's Guide to Wind Loading of Building Structures*, Butterworths, London.

Córdoba, G. (2005), A numerical model for the dynamics of pyroclastic flows at Galeras Volcano, Colombia, *J. Volcanol. Geotherm. Res.*, *139*, 59–71.

Dartevelle, S. (2004), Numerical modeling of geophysical granular flows: 1. A comprehensive approach to granular rheologies and geophysical multiphase flows, *Geochem. Geophys. Geosyst.*, *5*, Q08003, doi:10.1029/2003GC000636.

Dartevelle, S., W. I. Rose, J. Stix, K. Kelfoun, and J. W. Vallance (2004), Numerical modeling of geophysical granular flows: 2. Computer simulations of plinian clouds and pyroclastic flows and surges, *Geochem. Geophys. Geosyst.*, *5*, Q08004, doi:10.1029/2003GC000637.

Dellino, P., R. Isaia, L. La Volpe, and G. Orsi (2001), Statistical analysis of textural data from complex pyroclastic sequences: implications for fragmentation processes of the Agnano-Monte Spina Tephra (4.1 ka), Phlegrean Fields, southern Italy, *Bull. Volcanol.*, *63*, 433–461.

Dellino, P., R. Isaia, L. La Volpe, and G. Orsi (2004a), Interaction between particles transported by fallout and surge in the deposits of the Agnano-Monte Spina eruption (Campi Flegrei, Southern Italy), *J. Volcanol. Geotherm. Res.*, *133*, 193–210.

Dellino, P., R. Isaia, and M. Veneruso (2004b), Turbulent boundary layer shear flows as an approximation of base surges at Campi Flegrei (Southern Italy), *J. Volcanol. Geotherm. Res.*, *133*, 211–228.

de Vita, S., et al. (1999), The Agnano-Monte Spina eruption (4.1 ka) in the resurgent, nested Campi Flegrei caldera (Italy), *J. Volcanol. Geotherm. Res.*, *91*, 269–301.

Di Muro, A., A. Neri, and M. Rosi (2004), Contemporaneous convective and collapsing eruptive dynamics: The transitional regime of explosive eruptions, *Geophys. Res. Lett.*, *31*, L10607, doi:10.1029/2004GL019709.

Di Vito, M. A., L. Lirer, G. Mastrolorenzo, and G. Rolandi (1987), The Monte Nuovo eruption (Campi Flegrei, Italy), *Bull. Volcanol.*, *49*, 608–615.

Di Vito, M. A., R. Isaia, G. Orsi, J. Southon, S. de Vita, M. D'Antonio, L. Pappalardo, and M. Piochi (1999), Volcanic and deformational history of the Campi Flegrei caldera in the past 12 ka, *J. Volcanol. Geotherm. Res.*, *91*, 221–246.

Dobran, F., A. Neri, and G. Macedonio (1993), Numerical simulations of collapsing volcanic columns, *J. Geophys. Res.*, *98*, 4231–4259.

Dobran, F., A. Neri, and M. Todesco (1994), Assessing pyroclastic flow hazard at Vesuvius, *Nature*, *367*, 551–554.

D'Oriano, C., E. Poggianti, A. Bertagnini, R. Cioni, P. Landi, M. Polacci, and M. Rosi (2005), Changes in eruptive style during the A. D. 1538 Monte Nuovo eruption (Phlegrean Fields, Italy): The role of syn-eruptive crystallization, *Bull. Volcanol.*, *67*, 601–621.

Esposti Ongaro, T., A. Neri, M. Todesco, and G. Macedonio (2002), Pyroclastic flow hazard at Vesuvius from numerical modelling. II. Analysis of local flow variables, *Bull. Volcanol.*, *64*, 178–191.

Esposti Ongaro, T., A. Neri, C. Cavazzoni, G. Erbacci, A. Clarke, and B. Voight (2006), A new high-performance 3D multiphase flow code for the simulation of collapsing columns and volcanic blasts, paper presented at Cities on Volcanoes 4, IAVCEI, Quito, Ecuador, 23–27 Jan.

Fisher, R. V. (1990), Transport and deposition of pyroclastic surge across an area of high relief: The May 1980 eruption of Mount St Helens, Washington, *Geol. Soc. Am. Bull.*, *102*, 1038–1054.

Herzog, M., H. F. Graf, C. Textor, and J. M. Oberhuber (1998), The effects of phase change of water on the development of volcanic plumes, *J. Volcanol. Geotherm. Res.*, *87*, 55–74.

Isaia, R., M. D'Antonio, F. Dell'Erba, M. Di Vito, and G. Orsi (2004), The Astroni volcano: The only example of closely spaced eruptions in the same vent area during the recent history of the Campi Flegrei caldera (Italy), *J. Volcanol. Geotherm. Res.*, *133*, 171–192.

Ishimine, Y. (2005), Numerical study of pyroclastic surges, *J. Volcanol. Geotherm. Res.*, *139*, 33–57.

Kunii, D., and O. Levenspiel (1995), *Fluidization Engineering*, Elsevier, New York.

Lirer, L., P. Petrosino, and I. Alberico (2001), Hazard assessment at volcanic fields: The Campi Flegrei case history, *J. Volcanol. Geotherm. Res.*, *112*, 53–74.

Mason, P. J. (1994), Large-eddy simulation: a critical review of the technique, *Q. J. R. Meteorol. Soc.*, *120*, 1–26.

Neri, A., and F. Dobran (1994), Influence of eruption parameters on the thermofluid dynamics of collapsing volcanic columns, *J. Geophys. Res.*, *99*, 11,833–11,857.

Neri, A., and D. Gidaspow (2000), Riser hydrodynamics: Simulation using kinetic theory, *AIChE J.*, *46*, 52–67.

Neri, A., and G. Macedonio (1996), Numerical simulation of collapsing volcanic columns with particles of two sizes, *J. Geophys. Res.*, *101*, 8153–8174.

Neri, A., P. Papale, and G. Macedonio (1998), The role of magma composition and water content in explosive eruptions: II. Pyroclastic dispersion dynamics, *J. Volcanol. Geotherm. Res.*, *87*, 95–115.

Neri, A., P. Papale, D. Del Seppia, and R. Santacroce (2002), Couplet conduit and atmospheric dispersion dynamics during the Plinian phase of the AD 79 Vesuvius eruption, *J. Volcanol. Geotherm., Res.*, *120*, 141–160.

Neri, A., T. Esposti Ongaro, G. Macedonio, and D. Gidaspow (2003), Multiparticle simulation of collapsing volcanic columns and pyroclastic flow, *J. Geophys. Res.*, *108*(B4), 2202, doi:10.1029/2001JB000508.

Nuovo Colombo (1990), Carichi nelle costruzioni, manuale dell'ingegnere, Hoepli, Milan, Italy.

Oberhuber, J. M., M. Herzog, H. F. Graf, and K. Schwanke (1998), Volcanic plume simulation on a large scale, *J. Volcanol. Geotherm. Res.*, *87*, 29–53.

Orsi, G., S. de Vita, and M. Di Vito (1996), The restless, resurgent Campi Flegrei nested caldera (Italy): Constraints on its evolution and configuration, *J. Volcanol. Geotherm. Res.*, *74*, 179–214.

Orsi, G., M. Di Vito, and R. Isaia (2004), Volcanic hazard assessment at the restless Campi Flegrei caldera, *Bull. Volcanol.*, *66*, 514–530.

Ort, M. H., G. Orsi, L. Pappalardo, and R. V. Fisher (2003), Anisotropy of magnetic susceptibility studies of depositional processes in the Campanian Ignimbrite, Italy, *Bull. Volcanol.*, *65*, 55–72.

Papale, P. (2001), Dynamics of magma flow in volcanic conduits with variable fragmentation efficiency and nonequilibrium pumice degassing, *J. Geophys. Res.*, *106*, 11,043–11,065.

Papale, P. (2004), Simulation of eruptive scenarios at Phlegrean Fields based on field, laboratory and numerical studies and implication for volcanic hazard, Final Report of the INGV 2001–2003 Frame Program, Ist. Naz. di Geofis. e Vulcanol., Bologna, Italy.

Piochi, M., G. Mastrolorenzo, and L. Pappalardo (2005), Magma ascent and eruptive processes from textural and compositional features of Monte Nuovo pyroclastic products, Campi Flegrei, Italy, *Bull. Volcanol.*, *67*, 663–678.

Romano, C., D. Giordano, P. Papale, V. Mincione, D. B. Dingwell, and M. Rosi (2003), The dry and hydrous viscosities of silicate melts from Vesuvius and Phlegrean Fields, *Chem. Geol.*, *202*, 23–38.

Rosi, M., and R. Santacroce (1984), Volcanic hazard assessment in the Phlegraean Fields: A contribution based

on stratigraphic and historical data, *Bull. Volcanol.*, *47*, 359–370.

Rosi, M., and A. Sbrana (Eds.) (1987), *The Phlegrean Fields,* "*La Ricerca Scientifica*," vol. 114, Cons. Naz. delle Ric., Rome.

Rosi, M., A. Sbrana, and C. Principe (1983), The Phlegraean Fields: Structural evolution, volcanic history and eruptive mechanisms, *J. Volcanol. Geotherm. Res.*, *17*, 273–288.

Rossano, S., G. Mastrolorenzo, and G. De Natale (2004), Numerical simulation of pyroclastic density currents on Campi Flegrei topography: A tool for statistical hazard estimation, *J. Volcanol. Geotherm. Res.*, *132*, 1–14.

Sheridan, M. F., and M. C. Malin (1983), Application of computer assisted mapping to volcanic hazard evaluation of surge eruptions: Vulcano, Lipari and Vesuvius, *J. Volcanol. Geotherm. Res.*, *17*, 187–202.

Suzuki, Y. J., T. Koyaguchi, M. Ogawa, and I. Hachisu (2005), A numerical study of turbulent mixing in eruption clouds using a three-dimensional fluid dynamics model, *J. Geophys. Res.*, *110*, B08201, doi:10.1029/2004JB003460.

Todesco, M., A. Neri, T. Esposti Ongaro, P. Papale, G. Macedonio, R. Santacroce, and A. Longo (2002), Pyroclastic flow hazard at Vesuvius from numerical modelling. I. Large scale dynamics, *Bull. Volcanol.*, *64*, 155–177.

Valentine, G. A. (1998), Damage to structures by pyroclastic flows and surges, inferred from nuclear weapons effects, *J. Volcanol. Geotherm. Res.*, *87*, 117–140.

Valentine, G. A., and K. H. Wohletz (1989), Numerical models of Plinian eruption columns and pyroclastic flows, *J. Geophys. Res.*, *94*, 1867–1887.

Walker, J. P. L. (1981), The Waimihia and Hatepe Plinian deposits from the rhyolitic Taupo volcanic centre, N. Z. F., *Geol. Geophys.*, *24*, 305–324.